Research article

Journal of MASS SPECTROMETRY

Received: 2 June 2016 Revised: 8 September 2016 Accepted: 23 September 2016 Published online in Wiley Online Library

(wileyonlinelibrary.com) DOI 10.1002/jms.3889

# Theoretical investigation of low detection sensitivity for underivatized carbohydrates in ESI and MALDI

Jien-Lian Chen,[a] Chuping Lee,[a,b] I-Chung Lu,[a] Chia-Lung Chien,[a] Yuan-Tseh Lee,[a,b] Wei-Ping Hu[c] and Chi-Kung Ni[a,d]*

**Electrospray ionization (ESI) and matrix-assisted laser desorption/ionization (MALDI) mainly generate protonated ions from peptides and proteins but sodiated (or potassiated) ions from carbohydrates. The ion intensities of sodiated (or potassiated) carbohydrates generated by ESI and MALDI are generally lower than those of protonated peptides and proteins. Ab initio calculations and transition state theory were used to investigate the reasons for the low detection sensitivity for underivatized carbohydrates. We used glucose and cellobiose as examples and showed that the low detection sensitivity is partly attributable to the following factors. First, glucose exhibits a low proton affinity. Most protons generated by ESI or MALDI attach to water clusters and matrix molecules. Second, protonated glucose and cellobiose can easily undergo dehydration reactions. Third, the sodiation affinities of glucose and cellobiose are small. Some sodiated glucose and cellobiose dissociate into the sodium cations and neutral carbohydrates during ESI or MALDI process. The increase of detection sensitivity of carbohydrates in mass spectrometry by various methods can be rationalized according to these factors. Copyright © 2016 John Wiley & Sons, Ltd.**

*Additional supporting information may be found in the online version of this article at the publisher's web site.*

**Keywords:** carbohydrate; MALDI; ESI; low detection sensitivity

## Introduction

In the study of mass spectra of biomolecules by using electrospray ionization (ESI) and matrix-assisted laser desorption/ionization (MALDI), carbohydrates are significantly different from peptides and proteins. ESI and MALDI mainly generate protonated ions from peptides and proteins, although sodiated (or potassiated) peptides and proteins are occasionally generated.[1,2] By contrast, ESI and MALDI mainly generate sodiated (or potassiated) carbohydrates. For large carbohydrates, protonated carbohydrates are sometimes observed in ESI, but the intensity is low.[3,4] The ion intensities of sodiated and potassiated carbohydrates in ESI and MALDI are generally much lower than those of protonated peptides and proteins. The low ion intensity limits the applications of mass spectra to carbohydrate analysis.

Both the ion intensities obtained using ESI and MALDI are related to ion generation and release of ions from a solution or solid surface into the gas phase. Methylated carbohydrates are frequently used in mass spectrometry because of higher ionization efficiency than that of underivatized carbohydrates[3,5–8] and the applications in structure determination.[9] However, mass analysis of underivatized carbohydrates remains intensive investigation because of simple sample preparation.[10–13] It is worth investigating the properties which limits the ionization efficiency of underivatized carbohydrates. In this study, we focused on the stability of underivatized carbohydrate cations after the cations were generated. Glucose and cellobiose were studied as model molecules. We used the ab initio calculations and transition state theory (TST) to investigate the factors of low detection sensitivity for glucose and cellobiose in ESI and MALDI.

## Computational method

Geometries and relative energies of reactants, transition states and dissociation products were calculated using ab initio method. The molecular geometry and harmonic vibrational frequencies of the stationary points were calculated using B3LYP with the 6-311 + G (d,p) basis set. Single-point energies at the stationary points were calculated using the multilevel electronic structure method MCG3-MPWB[14], in which the geometries are calculated using B3LYP with the 6-311 + G(d,p) basis set. Thermal rate constants were calculated as a function of the temperature by using the conventional TST, except for the proton migration reaction. Because of the strong tunneling effect in the proton migration reaction, the rate constants of the proton migration reaction were calculated according to canonical variational theory with small-curvature tunneling approximation.[15,16] Electronic structure calculations were performed using the Gaussian 09 programs[17], and thermal

* *Correspondence to: Chi-Kung Ni, Department of Chemistry, National Tsing Hua University, Hsinchu 30013, Taiwan. E-mail: ckni@po.iams.sinica.edu.tw*

a *Institute of Atomic and Molecular Sciences, Academia Sinica, P. O. Box 23-166, Taipei 10617, Taiwan*

b *Department of Chemistry, National Taiwan University, Taipei 10617, Taiwan*

c *Department of Chemistry and Biochemistry, National Chung Cheng University, Chia-Yi 62102, Taiwan*

d *Department of Chemistry, National Tsing Hua University, Hsinchu 30013, Taiwan*

Journal of MASS SPECTROMETRY

rate constant calculations were performed using the Gaussrate 8.2 program[18], which is an interface between the Gaussian 09 and POLYRATE 8.2 programs.

## Results and discussion

### Glucose

*Protonated glucose*

The calculated proton affinity of α-glucose (α-D-glucopyranose in chair form) ranges from 187 to 202 kcal/mol, depending on the position of the attached proton. The geometries and relative energies of various protonated α-glucose isomers are shown in Fig. 1. The calculated proton affinities of glucose are similar to those reported in previous studies (198 kcal/mol).[19] Similar results were found for protonated β-glucose. Details are shown in Fig. S1 of Supporting Information. The barrier heights for isomerization from alpha form through open keto form to beta form are very low (12.6 kcal/mol), indicating the easy exchange between protonated glucose of alpha form and beta form. Details are shown in Fig. S2 of Supporting Information. The proton affinity of glucose is lower than that of most matrices used in MALDI, as listed in Table I of Supporting Information, except for α-cyano-4-hydroxycinnamic acid.[20,21] In particular, the proton affinity of glucose is lower than that of 2,5-dihydroxybenzoic acid (2,5-DHB) and 2,4,6-trihydroxyacetophenone, which are commonly used matrices for underivatized carbohydrates in MALDI.[3,5,22]

The proton affinity of water is lower than that of glucose.[23] Only the proton affinity of large water clusters $(H_2O)_n (n > 3)$ is higher than that of glucose.[23] We also calculated the geometries of protonated glucose–water clusters. The results indicate that the protons are attached to glucose when the number of water molecules is zero or one. However, the protons move toward water molecules when the number of water molecules increases ($n = 2, 3$). When the number of water molecules is 4, the protons are completely surrounded by water molecules. The trend indicates that the protons are enclosed by water molecules in the condensed phase and large glucose–water clusters. Details of calculation methods are shown in Supporting Information, and the geometries of protonated glucose–water clusters are shown in Fig. S4 of Supporting Information.

*Decomposition of protonated glucose*

After a proton attaches to glucose, it can migrate in glucose. Protonated glucose is converted from one isomer to other isomers because of the low barrier heights of proton migration. The proton migration barrier heights of protonated α-glucose (without water molecules) are shown in Fig. 1. The transition state geometries of isomerization are shown in Fig. S3(a) of Supporting Information.

Protonated glucose can easily be decomposed through the dehydration reaction, as shown by the low dissociation barriers in Fig. 1. The geometries of transition states and products are shown in Fig. S3(a) of Supporting Information. Among various protonated α-glucose isomers, α-PG1 has the lowest dissociation barrier. A similar low barrier height of the dehydration reaction for protonated glucose was reported.[24] Similar energy diagram but the barriers little higher than that of α-glucose was found for protonated β-glucose, as shown in Fig. S1 and S3(b) of Supporting Information.

The temperature-dependent rate constants of proton migrations and dehydration reactions of protonated glucose (without water molecules) were calculated using TST. The rate constants are listed in Table II of Supporting Information for the temperatures 300, 450, 600 and 1000 K. These temperatures correspond to the typical temperatures in ESI (300–650 K)[25] and MALDI (800–1500 K).[26] Calculations showed that the proton migration rate constants are higher than the dehydration reaction rate constants for most protonated glucose isomers, except for α-PG1. The results suggest that protonated glucose can easily be exchanged between these isomers before the dehydration reaction. However, the dehydration reaction rate constants of α-PG1 are large. These rate constants are higher than those of isomerization from α-PG1 to α-PG6 or from α-PG1 to α-PG2. After protonated glucose is isomerized to α-PG1, most of α-PG1 dissociates into fragments through the dehydration

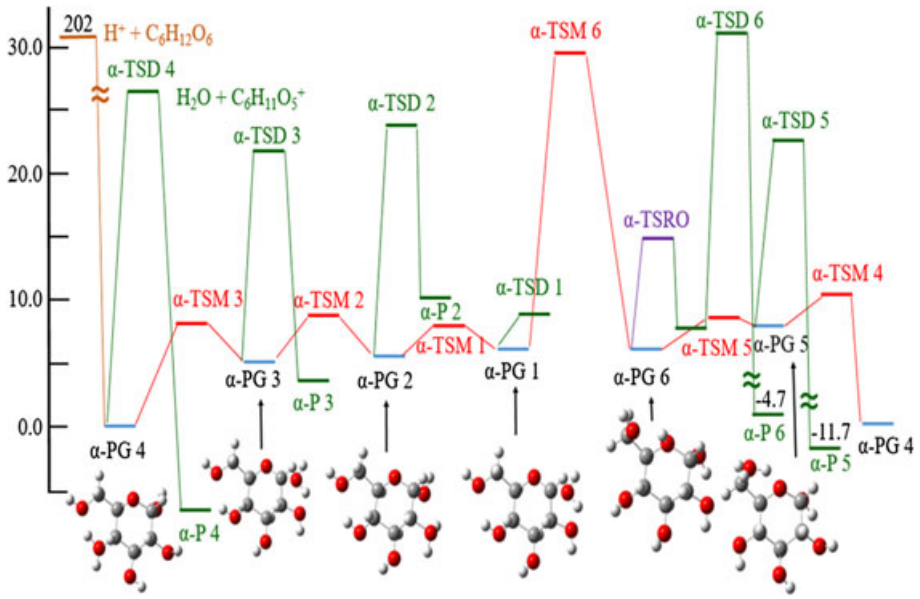


**Figure 1.** Geometries and relative energies (in kcal/mol) of protonated glucose (α-D-glucopyranose in chair form) and barrier heights of proton migration (red dashed line) and dehydration reactions (green dashed line). The geometries of transition states and products are shown in Supporting Information. Similar barrier heights of isomerization and dehydration for β-glucose were found; details are shown in Supporting Information.



  

reaction. The population decay of α-PG1 resulting from the dehydration reaction can easily be compensated by the population transfer from the other isomers. Similar trend but smaller dissociation rates were found for β-glucose. According to our calculations, 50% population decay of protonated α-glucose (β-glucose) takes 1 μs (20 ms), 15 ns (2 μs), 1 ns (15 ns) and 20 ps (20 ps) at the temperatures 300, 450, 600 and 1000 K, respectively. Details of the calculations are shown in Supporting Information.

The proton affinity of the product of the dehydration reaction, $C_6H_{11}O_5^+$, is 198 kcal/mol, which is lower than that of glucose, most matrices used in MALDI and water clusters. A part of the dehydration products may transfer the protons to the surrounding molecules (matrix or water) and becomes a neutral species. A part of the dehydration products may undergo a sequential dehydration reaction. The barrier heights of both proton migration in $C_6H_{11}O_5^+$ and the sequential dehydration reaction, $C_6H_{11}O_5^+ \rightarrow C_6H_9O_4^+ + H_2O$, are very low, as illustrated in Fig. 2. The rate constants of proton migration and the dehydration reaction are listed in Table III of Supporting Information. According to the calculations, 50% population decay of the dehydration product, $C_6H_{11}O_5^+$, takes 500 ms, 2 μs, 20 ns and 200 ps through further dehydration reaction at the temperatures 300, 450, 600 and 1000 K, respectively.

The proton affinity of the product of the second dehydration reaction, $C_6H_9O_4^+$, is further reduced to 196 kcal/mol. A part of the dehydration product may undergo a proton transfer reaction and become a neutral species. The third water molecule elimination, $C_6H_9O_4^+ \rightarrow C_6H_7O_3^+ + H_2O$, also has a low barrier height. The barrier heights of proton migration in $C_6H_9O_4^+$ and the dehydration reaction are illustrated in Fig. 3. The rate constants of proton migration and the dehydration reaction are listed in Table IV of Supporting Information. According to the calculations, 50% population decay of $C_6H_9O_4^+$ takes 200 ms, 25 μs, 150 ns and 100 ps at the temperatures 300, 450, 600 and 1000 K, respectively.

The proton affinity of the product of the third dehydration reaction, $C_6H_7O_3^+$, is further reduced to 182 kcal/mol, which is very low. Hence, a proton transfer reaction can easily occur. We found that further decomposition of $C_6H_7O_3^+$ is related to ring opening dissociation. The barrier heights of the ring opening dissociation channels of $C_6H_7O_3^+$ are high (>60 kcal/mol). Ring opening dissociation can occur only at a much higher temperature.

Previous paragraphs describe the dehydration reaction of protonated glucose (without water molecules). For protonated glucose–water clusters, proton attaches to glucose only when the number of water molecules is one. Therefore, dehydration reaction only occurs for glucose–water clusters when the number of water molecules is one. We did not calculate the dehydration reaction of protonated glucose–water ($n = 1$) cluster because there are too many dissociation pathways. The search of minimum barrier height for dehydration reactions of protonated glucose–water clusters is beyond the scope of this manuscript. However, if the dehydration reaction of protonated glucose with one water molecule occurs, it increases the overall dehydration reaction rate of protonated glucose. This enhances our conclusion: protonated glucose easily undergoes dehydration reaction.

### *Sodiated glucose*

The sodiation affinity of α-glucose ranges from 36.4 to 45 kcal/mol, depending on the position of the attached sodium, as illustrated in Fig. 4. Similar sodiation affinity (44 kcal/mol) of glucose has been reported.[27] In contrast to the proton affinity of glucose, which is lower than that of matrices, the sodiation affinity of glucose is higher than that of matrices. The sodiation affinities of glucose and various matrices are listed in Table I of Supporting Information. Similar to the proton migration reaction in glucose, the sodium atom can also migrate in glucose, as shown by the low barriers of sodium migration. The transition state geometries of sodium migration are shown in Fig. S10 of Supporting Information.

### *Decomposition of sodiated glucose*

Protonated glucose can easily undergo the dehydration reaction. However, the analogous dissociation channel of sodiated glucose, namely NaOH elimination, $C_6H_{12}O_6Na^+ \rightarrow C_6H_{11}O_5^+ + NaOH$, has a

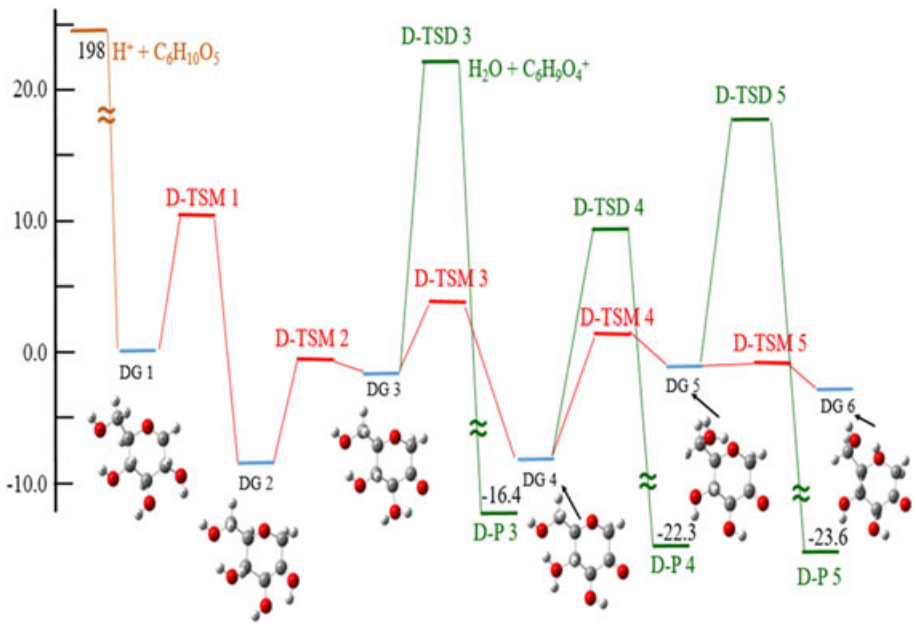


**Figure 2.** Geometries and relative energies (in kcal/mol) of $C_6H_{11}O_5^+$ and barrier heights of proton migration (red) and dehydration reactions (green). The geometries of transition states are shown in Figure S5 of Supporting Information.

Journal of MASS SPECTROMETRY

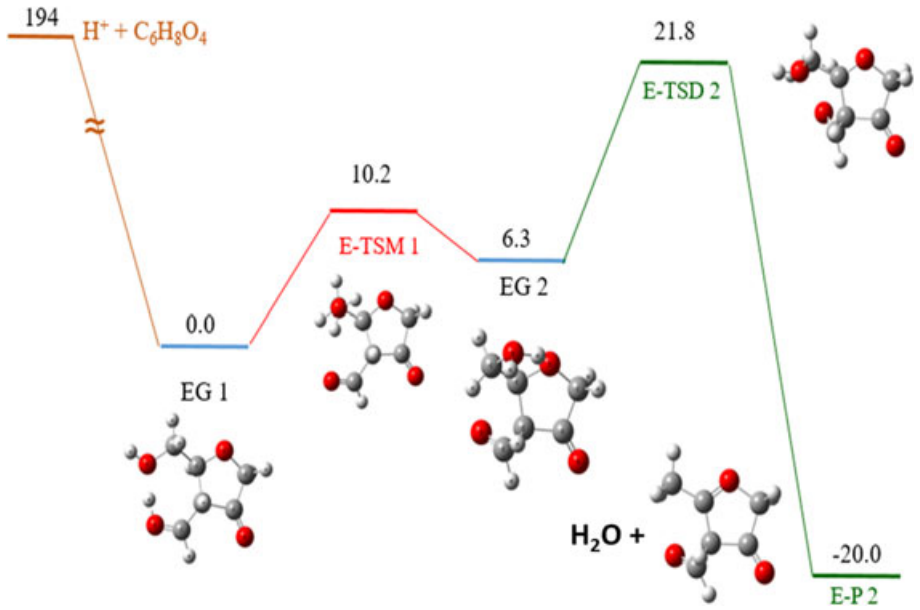


**Figure 3.** Geometries and relative energies (in kcal/mol) of $C_6H_9O_4^+$ and barrier heights of proton migration (red) and the dehydration reaction (green).

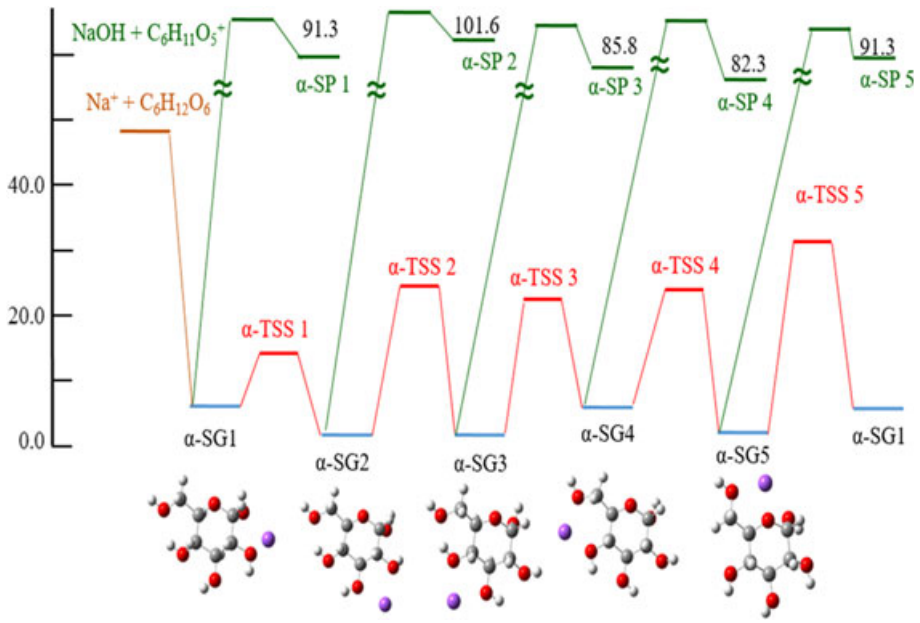


**Figure 4.** Geometries and relative energies (in kcal/mol) of sodiated α-glucose and barrier heights of sodium migration (red). NaOH elimination is plotted in green, and only the product energies are plotted in scale. The barrier heights of NaOH elimination are not calculated, and they are not plotted in scale. Because the barrier of NaOH elimination must be equal or larger than the product energies, large heat of reaction of NaOH elimination ensures that NaOH elimination does not occur. Calculations of barrier heights are not necessary. Similar energy diagram was found for sodiated β-glucose, as shown in Figure S9 of Supporting Information.

large heat of reaction. Figure 4 shows the heat of reactions for NaOH elimination. Because the barrier height of NaOH elimination must be equal or larger than the heat of reaction, the large heat of reaction of NaOH elimination ensures that this analogous dehydration reaction is not expected to occur. Instead, sodiated glucose at a high temperature undergoes the desodiation reaction $C_6H_{12}O_6Na^+ \rightarrow C_6H_{12}O_6 + Na^+$ because of the low sodiation affinity.

The temperature-dependent rate constants of sodium migration and desodiation reactions are shown in Table V of Supporting Information. The rate constants of sodium migration are higher than those of desodiation, indicating that the sodium cation migrates in glucose before sodiated glucose decomposes into glucose and the sodium cation. According to the calculations, 50% population decay of sodiated α-glucose (β-glucose) takes 200 ns (800 ms) and 0.3 ns (20 ns) through the desodiation reaction at the temperatures 600 and 1000 K, respectively.

### Cellobiose

The proton affinity of cellobiose ranges from 197 to 222 kcal/mol, depending on the position of the attached proton. The proton affinity of cellobiose is higher than that of glucose. The proton affinity is



  

sufficiently high for cellobiose to compete with matrices for protons. The barrier heights of dehydration reactions range from 23 to 42 kcal/mol, which are only slightly higher than those of glucose. The low barrier heights of dehydration reactions indicate that after a proton attaches to cellobiose, the dehydration reaction can easily occur. Among various dehydration reaction channels, the dehydration of the glycosidic linkage, $C_{12}H_{22}O_{11}H^+ \rightarrow C_6H_{11}O_5^+ + C_6H_{12}O_6$, has the lowest barrier height (23 kcal/mol). After the cleavage of the glycosidic linkage, the product, $C_6H_{11}O_5^+$, can easily undergo a sequential dehydration reaction, as described for protonated glucose. The dehydration of the hydroxyl group connected to the carbon atom at position 3 of cellobiose, $C_{12}H_{22}O_{11}H^+ \rightarrow C_{12}H_{20}O_{10}H^+ + H_2O$, has the second lowest barrier height (25.8 kcal/mol). This dehydration reaction competes with the cleavage of the glycosidic linkage.

The sodiation affinity of cellobiose (63 kcal/mol) is higher than that of glucose (45 kcal/mol). However, it is still much lower than the proton affinity of cellobiose. By contrast, the barrier heights of the dissociation channel analogous to the dehydration reaction of protonated glucose decrease to 63 kcal/mol for $C_{12}H_{22}O_{11}Na^+ \rightarrow C_{12}H_{21}O_{10}^+ + NaOH$, 61 kcal/mol for $C_{12}H_{22}O_{11}Na^+ \rightarrow C_6H_{12}O_6 + C_6H_{10}O_5Na^+$ and 59 kcal/mol for $C_{12}H_{22}O_{11}Na^+ \rightarrow C_6H_{12}O_6Na^+ + C_6H_{10}O_5$. The barrier heights of the desodiation reaction and the reactions analogous to dehydration reactions are similar (59–63 kcal/mol). These reactions may occur and compete with each other at a high temperature. Details of calculation of protonated cellobiose and sodiated cellobiose are shown in Supporting Information.

### Stability of carbohydrate cations in MALDI

Most of the protons produced by MALDI attach to matrices, but not glucose. This is because the proton affinity of glucose is lower than that of matrices, and the matrix concentration is much higher than that of glucose. Even if a small amount of protons attaches to glucose (e.g. the partial equilibrium between reactants and products), our calculations show that protonated glucose rapidly dissociates into fragments because of the high temperature (800–1500 K) during MALDI. The dehydration reaction is followed by the sequential dehydration reaction or the proton transfer reaction, $C_6H_{11}O_5^+ + M \rightarrow C_6H_{10}O_5 + MH^+$ (M represents the matrix), because of the low proton affinity of $C_6H_{10}O_5$. Similar dehydration and proton transfer reactions can occur after the second water elimination. The reduction of total protonated glucose (including various isomers) at 1000 K is extremely rapid; calculations of dissociation rate show that most of the protonated glucose dissociates into fragments within 1 ns. The time required for dissociation is much shorter than the high temperature duration in MALDI (<100 ns) [26]. This property is very different from those of peptides and proteins. The proton affinities of peptides and proteins are higher than those of matrices, and protonated peptides and protonated proteins do not easily dissociate into fragments. The relative low proton affinity with respect to the MALDI matrix and the rapid decomposition of protonated glucose and protonated dehydration products explain why no protonated glucose and protonated dehydration products are observed in MALDI.

Cellobiose has a higher proton affinity than that of matrices. Cellobiose can compete with matrix for protons. However, the barrier height of the dehydration reaction is low, and protonated cellobiose easily undergoes dehydration reactions. These dehydration reactions reduce the cellobiose detection sensitivity.

Sodium cations produced by MALDI attach to glucose or cellobiose instead of matrices, because the sodiation affinity of glucose and cellobiose are higher than those of the matrix. In MALDI experiment, sodiated matrix is frequently observed. If the amount of sodium cations is more than that of glucose or cellobiose in a MALDI sample, the extra sodium cations may attach to matrix molecules. The sodiation affinity of glucose (or cellobiose) is lower than the proton affinity of glucose (or cellobiose); sodiated glucose and cellobiose can decompose back to the reactants (sodium cations and glucose or cellobiose) owing to the high temperature during MALDI process. According to our calculations of dissociation rate, the dissociation of sodiated glucose takes 20 ns (1000 K), which is in a similar order of magnitude to that of the high temperature duration in MALDI. Consequently, some sodiated glucose must decompose into glucose and the sodium cations. The decomposition reduces the detection sensitivity for sodiated glucose in MALDI.

### Stability of carbohydrate cations in ESI

Our calculations show that protons in the droplet are surrounded by water molecules. Proton attaches to glucose and dehydration reaction occurs only when most of the water molecules vaporize. The calculated dehydration reaction rate shows that 50% population decay of protonated glucose takes only 20 ms and 15 ns at 300 and 600 K, respectively. The dehydration product, $C_6H_{11}O_5^+$, may undergo sequential dehydration, resulting in $C_6H_9O_4^+$ and $C_6H_7O_3^+$. According to our calculations, the second dehydration reaction takes 500 ms and 20 ns, and the third dehydration reaction takes 200 ms and 150 ns at 300 and 600 K, respectively. The products from the dehydration reactions are observed in ESI mass spectra, as illustrated in Fig. 5(a) and 5(b). The relative ion intensities of $m/z = 127$ (product of the third dehydration reaction) and $m/z = 145$ (product of the second dehydration reaction) increase as the temperature increases. The trend is consistent with the theoretical prediction. The rapid dehydration reactions cause the detected ion intensity of protonated glucose to be low in ESI. Dehydration reactions are also observed in cellobiose and in large carbohydrates such as maltopentaose, as shown in the Supporting Information of Fig. S12(a) and Fig. S13(a).

The ion intensity of sodiated glucose increases rapidly as the concentration of sodium cations in the solution increases, as illustrated in Fig. 5(c). This is because sodiated glucose is much more stable than protonated glucose. According to our calculations, sodiated glucose can decompose into neutral glucose and the sodium cation. The decomposition of 50% sodiated glucose takes 800 ms (600 K), which is comparable to the duration of ions in ESI. The decomposition reduces the detection sensitivity for sodiated glucose generated by ESI.

The sodiated cellobiose has three dissociation channels which the barrier heights are similar to that of desodiation reaction. These three dissociation channels are $C_{12}H_{22}O_{11}Na^+ \rightarrow C_{12}H_{21}O_{10}^+ + NaOH$, $C_{12}H_{22}O_{11}Na^+ \rightarrow C_6H_{12}O_6 + C_6H_{10}O_5Na^+$ and $C_{12}H_{22}O_{11}Na^+ \rightarrow C_6H_{12}O_6Na^+ + C_6H_{10}O_5$. The decomposition barrier heights of sodiated cellobiose are slightly higher than those of glucose; however, the decomposition of sodiated cellobiose is still observed, as shown by the ion $m/z = 325$, 203 and 185 in the Supporting Information of Fig. S12(b).

### Methods for improving carbohydrate detection sensitivity

By understanding the factors causing the low detection sensitivity for carbohydrates, methods proposed for increasing the detection sensitivity in previous studies can be rationalized.

Journal of MASS SPECTROMETRY

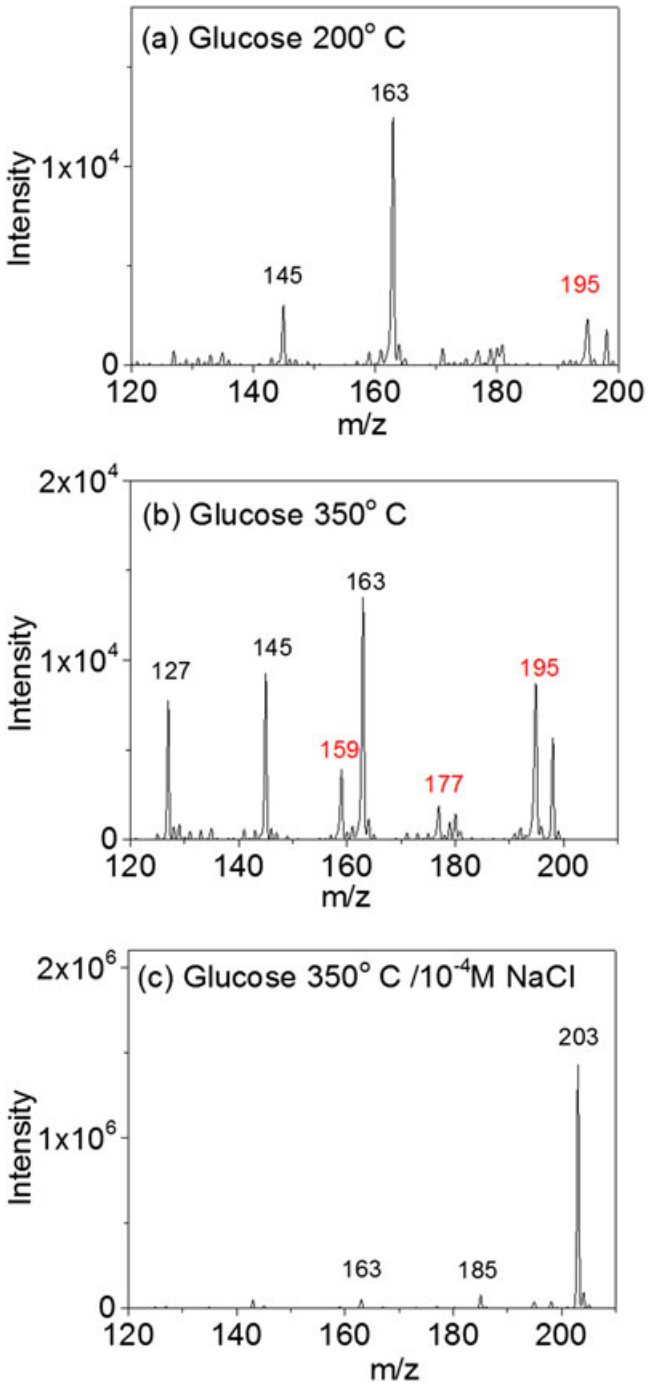


**Figure 5.** ESI mass spectra of glucose. (a) and (b): Solution containing $10^{-3}$ M glucose in a 1:1 water/methanol solvent. (c): Solution containing $10^{-3}$ M glucose and $10^{-4}$ M NaCl in a 1:1 water/methanol solvent. Ion $m/z = 163$, 145 and 127 represent the dehydration products of protonated glucose, $C_6H_{13}O_6^+ \rightarrow C_6H_{13-2n}O_{6-n}^+ + (H_2O)_n$ for $n = 1$, 2 and 3. Ion $m/z = 195$, 177 and 159 represent a methanol molecule (from solution) attached to the dehydration products. Ion $m/z = 203$ represents sodiated glucose, and $m/z = 185$ represents the sodiated glucose after water elimination. Details of experimental conditions are shown in Supporting Information.

In MALDI, desorption occurs only at a high temperature. However, a high temperature results in the decomposition of protonated and sodiated carbohydrates. The dehydration barrier height of protonated carbohydrates is extremely low; hence, it is not likely that carbohydrates can be desorbed from the solid state into the gas phase at a temperature without the decomposition of protonated carbohydrates. However, the desodiation energy is much higher than the barrier height of the dehydration reaction. The temperature can be reduced to maintain desorption; meanwhile, decomposition of sodiated carbohydrates is reduced. A study demonstrated that a frozen solution at 100 K generates more sodiated carbohydrate ions.[28] The frozen sample mainly comprises water and acetonitrile, and a small amount of 2,5DHB and analyte. UV photons of laser pulses irradiating on the frozen sample are absorbed by 2,5-DHB. 2,5-DHB changes the photon energy into thermal energy by internal conversion, followed by the energy transfer to surrounding molecules. The melting points and boiling points of water and acetonitrile are much lower than those of the matrices in typical MALDI dried droplet sample. Molecules can be desorbed into the gas phase at a much lower temperature from frozen solution than that of the matrix. The sodiated carbohydrate ion generation efficiency of a frozen solution at 100 K is 20–30 times higher than that of a conventional dried droplet at room temperature. The low temperature facilitates reducing the decomposition of sodiated carbohydrates and increases the ion generation efficiency.

Another method for increasing the carbohydrate detection sensitivity is the addition of a small fraction of salt to the ESI solution. Instead of using residual sodium ions from an impure solution, adding a small amount of salt provides a large and stable sodiated ion signal. Figure 5 and Figs S12 and S13 of Supporting Information show that the detection sensitivities for glucose, cellobiose and maltopentaose increase by a factor of 10–50 when a small amount of NaCl is added to the ESI solution. Adding a small amount of NaCl or LiCl in ESI solution to increase the detection sensitivity has been reported in previous studies.[29,30]

Comparison of glucose and cellobiose shows that both the proton affinity and sodiation affinity increase as the size of the carbohydrate increases. This is because the number of hydroxyl groups of carbohydrate interacting with the proton or sodium ion increases. In addition, calculations according to TST suggest that the dissociation rate of the dehydration reaction for large carbohydrates is slower than small carbohydrates because of the large number of vibrational degrees of freedom. Consequently, large protonated carbohydrates do not undergo the dehydration reaction completely; some of the protonated carbohydrate can be observed in ESI mass spectra, as shown in Fig. S13(a) of Supporting Information for maltopentaose. However, the ion intensity of protonated maltopentaose remains much lower than that of sodiated carbohydrates when a small amount of salt is added to the ESI solution, as illustrated in Fig. S13(b).

#### Acknowledgements

We acknowledge the support of the Thematic Research Program, Academia Sinica, Taiwan (AS-102-TP-A08) and the Ministry of Science and Technology, Taiwan (NSC 100-2113-M-001-026-MY3).

## References

[1] K. Hjerno, O. N. Jensen. MALDI-MS in protein chemistry and proteomics. In *MALDI-MS A Practical Guide to Instrumentation Method and Applications*(F. Hillenkamp, J. Peter-Katalinic Eds.). Wiley-VCH Verlag GmbH & Co. KGaA: Weinheim, **2007**.

[2] J. A. Loo, R. R. O. Loo. Electrospray ionization mass spectrometry of peptides and proteins. In *Electrospray Ionization Mass Spectrometry, Fundamentals Instrumentation & Applications*(R. B. Cole Ed.). John Wiley & Son, Inc.: New York, **1997**.

[3] D. Sagi, J. Peter-Katalinic. MALDI-MS of Glycans. In *MALDI-MS A Practical Guide to Instrumentation Method and Applications*(F. Hillenkamp, J.



  

Peter-Katalinic Eds.). Wiley-VCH Verlag GmbH & Co. KGaA: Weinheim, **2007**.
[4] Y. Ohashi. Electrospray ionization mass spectrometry of carbohydrates and lipids. In *Electrospray Ionization Mass Spectrometry, Fundamentals Instrumentation & Applications*(R. B. Cole Ed.). John Wiley & Son, Inc.: New York, **1997**.
[5] D. J. Harvey. Matrix-assisted laser desorption ionization mass spectrometry of carbohydrates. *Mass Spectrom. Rev.* **1999**, *18*, 349–451.
[6] J. Zaia. Mass spectrometry of oligosaccharides. *Mass Spectrom. Rev.* **2004**, *23*, 161–227.
[7] S. Hakomori. A rapid permethylation of glycolipid and polysaccharide catalyzed by methylsulfinyl carbanion in dimethyl sulfoxide. *J. Biochem. (Tokyo)* **1964**, *55*, 205–208.
[8] I. Ciucanu, F. Kerek. A simple and rapid method for the permethylation of carbohydrates. *Carbohydr. Res.* **1984**, *131*, 209–217.
[9] D. Ashline, S. Singh, A. Hanneman, V. Reinhold. Congruent strategies for carbohydrate sequencing. 1. Mining structural details by $MS^n$. *Anal. Chem.* **2005**, *77*, 6250–6262.
[10] T. Yamagaki1, H. Nakanishi. Post-source decay fragmentation analyses of linkage isomers of Lewis-type oligosaccharides in curved-field reflectron matrix-assisted laser desorption/ionization time-of-flight mass spectrometry: combined in-source decay/post-source decay experiments and relative ion abundance analysis. *J. Mass Spectrom.* **2000**, *35*, 1300–1307.
[11] J. Simoes, P. Domingues, A. Reis, F. M. Nunes, M. A. Coimbra, M. R. M. Domingues. Identification of anomeric configuration of underivatized reducing glucopyranosyl-glucose disaccharides by tandem mass spectrometry and multivariate analysis. *Anal. Chem.* **2007**, *79*, 5896–5905.
[12] A. Kuki, K. E. Szabo, L. S. Nagy, M. Zsuga, S. Keki. Rapid identification of disaccharides by tandem mass spectrometry. *J. Mass Spectrom.* **2013**, *48*, 1276–1280.
[13] P. Both, A. P. Green, C. J. Gray, R. S. Ardzk, J. Voglmeir, C. Fontana, M. Austeri, M. Rejzek, D. Richardson, R. A. Field, G. Widmalm, S. L. Flitsch, C. E. Eyers. Discrimination of epimeric glycans and glycopeptides using IM-MS and its potential for carbohydrate sequencing. *Nat. Chem.* **2014**, *6*, 65–74.
[14] Y. Zhao, B. J. Lynch, D. G. Truhlar. Multi-coefficient extrapolated density functional theory for thermochemistry and thermochemical kinetics. *Phys. Chem. Chem. Phys.* **2005**, *7*, 43–52.
[15] Y.-P. Liu, G. C. Lynch, T. N. Truong, D.-H. Lu, D. G. Truhlar, B. C. Garrett. Molecular modeling of the kinetic isotope effect for the [1,5]-sigmatropic rearrangement of cis-1,3-pentadiene. *J. Am. Chem. Soc.* **1993**, *115*, 2408–2415.
[16] D.-H. Lu, T. N. Truong, V. S. Melissas, G. C. Lynch, Y.-P. Liu, B. C. Garrett, R. Steckler, A. D. Isaacson, S. N. Rai, G. C. V. Hancock, J. G. Lauderdale, T. Joseph, D. G. Truhlar. POLYRATE 4: a new version of a computer program for the calculation of chemical reaction rates for polyatomics. *Comput. Phys. Commun.* **1992**, *71*, 235–262.
[17] M. J. Frisch, G. W. Trucks, H. B. Schlegel, G. E. Scuseria, M. A. Robb, J. R. Cheeseman, G. Scalmani, V. Barone, B. Mennucci, G. A. Petersson, H. Nakatsuji, M. Caricato, X. Li, H. P. Hratchian, A. F. Izmaylov, J. Bloino, G. Zheng, J. L. Sonnenberg, M. Hada, M. Ehara, K. Toyota, R. Fukuda, J. Hasegawa, M. Ishida, T. Nakajima, Y. Honda, O. Kitao, H. Nakai, T. Vreven, J. A. Montgomery Jr., J. E. Peralta, F. Ogliaro, M. Bearpark, J. J. Heyd, E. Brothers, K. N. Kudin, V. N. Staroverov, R. Kobayashi, J. Normand, K. Raghavachari, A. Rendell, J. C. Burant, S. S. Iyengar, J. Tomasi, M. Cossi, N. Rega, J. M. Millam, M. Klene, J. E. Knox, J. B. Cross, V. Bakken, C. Adamo, J. Jaramillo, R. Gomperts, R. E. Stratmann, O. Yazyev, A. J. Austin, R. Cammi, C. Pomelli, J. W. Ochterski, R. L. Martin, K. Morokuma, V. G. Zakrzewski, G. A. Voth, P. Salvador, J. J. Dannenberg, S. Dapprich, A. D. Daniels, Ö. Farkas, J. B. Foresman, J. V. Ortiz, J. Cioslowski, D. J. Fox. *Gaussian 09, Revision E.01*. Gaussian, Inc: Wallingford CT, **2009**.
[18] J. C. Corchado, Y.-Y. Chunag, E. L. Coitino, D. G. Truhlar. *Gaussrate, version 8.2*. University of Minnesota: Minneapolis, MN, **1999**.
[19] K. A. Jabber, K. Zhang, C. J. Cassady, A. Chung-Phillips. Ab initio and experimental studies on the protonation of glucose in the gas phase. *J. Am. Chem. Soc.* **1996**, *118*, 10515–10524.
[20] E. Schulz, M. Karas, F. Rosu, V. Gabelica. Influence of the matrix on analyte fragmentation in atmospheric pressure MALDI. *J. Am. Soc. Mass Spectrom.* **2006**, *17*, 1005–1013.
[21] S. P. Mirza, N. P. Raju, M. Vairamani. Estimation of the proton affinity values of fifteen matrix-assisted laser desorption/ionization matrices under electrospray ionization conditions using the kinetic method. *J. Am. Soc. Mass Spectrom.* **2004**, *15*, 431–435.
[22] N.-Y. Hsu, W.-B. Yang, C.-H. Wong, Y.-C. Lee, R.-T. Lee, Y.-S. Wang, C.-H. Chen. Matrix-assisted laser desorption/ionization mass spectrometry of polysaccharides with 2′,4′,6′-trihydroxyacetophenone as matrix. *Rapid Commun. Mass Spectrom.* **2007**, *21*, 2137–2146.
[23] Y. Kawai, S. Yamaguchi, Y. Okada, K. Takeuchi, Y. Yamauchi, S. Ozawa, H. Nakai. Reactions of protonated water clusters $H^+(H_2O)n$ ($n = 1–6$) with dimethylsulfoxide in a guided ion beam apparatus. *Chem. Phys. Lett.* **2003**, *377*, 69–73.
[24] X. Lin, Y. Qu, Y. Le, Y. Xi, D. L. Phillips, C. Liu. The first dehydration and the competing reaction pathways of glucose homogeneously and heterogeneously catalyzed by acids. *Phys. Chem. Chem. Phys.* **2013**, *15*, 2967–2982.
[25] For example, LTQ XLSeries Getting Start Guide, 97055-97073 Revision A, **2009**, Thermo Fisher Scientific Inc.
[26] A. Koubenakis, V. Frankevich, J. Zhang, R. Zenobi. Time-resolved surface temperature measurement of MALDI matrices under pulsed UV laser irradiation. *J. Phys. Chem. A* **2004**, *108*, 2405–2410.
[27] A. L. Heaton, P. B. Armentrout. Experimental and theoretical studies of sodium cation interactions with D-arabinose, xylose, glucose, and galactose. *J. Phys. Chem. A* **2008**, *112*, 10156–10167.
[28] C. W. Liang, P. J. Chang, Y. J. Lin, Y. T. Lee, C. K. Ni. High ion yields of carbohydrates from frozen solution by UV-MALDI. *Anal. Chem.* **2012**, *84*, 3493–3499.
[29] M. R. Asam, G. L. Glish. Tandem mass spectrometry of alkali cationized polysaccharides in a quadrupole ion trap. *J. Am. Soc. Mass Spectrom.* **1997**, *8*, 987–995.
[30] B. Quéméner, M. C. Ralet. Evidence for linkage position determination in known feruloylated mono-and disaccharides using electrospray ion trap mass spectrometry. *J. Mass Spectrom.* **2004**, *39*, 1153–1160.

## Supporting information

Additional supporting information may be found in the online version of this article at the publisher's web site.